Ab Initio Simulation of Lewis Sites in Mordenite and Comparative Study of the Strength of Active Sites via CO Adsorption

L. Benco,*,†,‡ T. Bucko,† J. Hafner,† and H. Toulhoat§

Institut für Materialphysik and Center for Computational Materials Science, Universität Wien, Sensengasse 8, A-1090 Wien, Austria, Institute of Inorganic Chemistry, Slovak Academy of Sciences, Dubravska cesta 9, SK-84236 Bratislava, Slovak Republic, and Institut Français du Pétrole, F-92852 Rueil-Malmaison Cedex, France

Received: May 6, 2004; In Final Form: June 24, 2004

Ab initio density-functional investigations of intrazeolite active centers have been performed for mordenite. We investigate the structure and properties of bare Al^{3+} cations bound to the framework and originating from extra-framework $Al(H_2O)_6^{3+}$ cations dehydrated at severe thermal treatment of the zeolite. A bare Al^{3+} cation in the zeolite causes either a limited local relaxation or is trapped in a small ring of the zeolite structure without substantial relaxation of the framework. Such a cation behaves as a strong Lewis site. The strength of trapped Al^{3+} is evaluated via the adsorption of CO and compared to a variety of zeolite active centers such as Brønsted sites, Na-counterions, and surface silanols. An overall agreement between experimental and calculated shifts of the CO stretching frequency is observed. The comparison of bare and hydrated Al^{3+} and Ga^{3+} cations shows that stretching frequencies blue-shifted to $\sim$2230 cm^{-1} can originate only from adsorption on bare cations. In zeolites not containing any exchanged extra-framework cations the presence of stretching bands at $\sim$2230 thus cm^{-1} evidences the presence of highly active bare Al^{3+} trapped in five-membered rings of the zeolite framework.

1. Introduction

Zeolites are catalysts with active sites that act as proton donors (Brønsted acids). The H-forms of zeolites are solid acids with many industrial applications. The importance of Brønsted acid sites for chemical conversion processes is evidenced by a huge amount of experimental material showing a direct correlation between the concentration of acid sites and the conversion rate. Besides the Brønsted acidity of the H-form, zeolites also contain cations and admixtures that can accept electron pairs, thus acting as Lewis acids. Extra-framework aluminum particles (EFAL), derived either from aluminum oxide particles not consumed during the synthesis or from Al-oxides released during the dealumination of the framework, appear to be a natural component of zeolites. Other metallic cations of metals, such as Ga, Fe, Zn, Cu, and Pt, can be introduced into zeolites by ion exchange, replacing the Na or Ca cations present in natural zeolites. Continued growth of experimental material demonstrates the importance of Lewis centers for intrazeolite reactivity. An increasing number of studies therefore focus on a better characterization of the Lewis sites. Gola et al.[1] have identified and quantified EFAL particles in stabilized Y zeolite. An investigation of the nature of EFAL species in USY has been reported by Omegna et al..[2,3] The relation between framework and extra-framework Al and the catalytic performance of Pt/USY catalysts was studied by Arribas and Martínez.[4] They found that the concentration of EFAL relates to the total acidity of the catalyst which determines the product yield and selectivity of the conversion. The EFAL particles thus seem to play an important role in the intrazeolite chemistry.

The deposition of metal ions in zeolite matrixes has been intensively studied using computational methods. The structure and the coordination of EFAL particles deposited in Y zeolite as cations (Al^{3+}, $Al(OH)^{2+}$, AlO^{+}, $Al(OH)_2^{+}$) or neutral particles (AlO(OH), $Al(OH)_3$) has recently been reported by Bhering et al.[5] Most theoretical studies, however, investigate the deposition of transition-metal ions such as Pd[6] and Cu,[7−10] but also other metals active in catalytic conversions such as Zn[11−14] and Zn−O−Zn clusters.[15,16] A variety of structural models have been considered, and different theoretical methods have been applied. Most frequently small model clusters are used to mimic zeolite structures.[9−11,13−15] Recently the application of modern periodical approaches, based on density-functional theory, has been extended to complex zeolite structures and is increasingly applied to study intrazeolite deposition of metal ions.[6,12,16] A variety of zeolite structures are under study, including the small cell zeolite chabazite,[12,16] the medium cell zeolite gmelinite,[6] and the large cell zeolites ZSM5 and faujasite.[7−10,14]

In our recent work we have studied the dynamical behavior of small neutral EFAL particles occluded in both the channel and the cage of a zeolite.[17] The EFAL particle is represented by hydrated aluminum hydroxide. In the zeolite, neutral EFAL particles are only weakly physisorbed. Frequent transfers of acid protons from the zeolite to the occluded particle indicate rather strong Brønsted basicity of such particles. Because no tendency to a proton attack at adsorbed hydrocarbon molecules is observed, we have concluded that neutral EFAL species are not active in processes of intrazeolite hydrocarbon conversion.

In the present work an up-to-date periodic density-functional method is applied to investigate the behavior of a bare noncoordinated Al^{3+} cation deposited in the industrially im-

* Corresponding author. Tel.: +43-1-4277-51407. Fax.: +43-1-4277-9413. E-mail: lubomir.benco@univie.ac.at.
† Universität Wien.
‡ Slovak Academy of Sciences.
§ Institut Français du Pétrole.

10.1021/jp048056t CCC: $27.50
Published on Web 08/13/2004

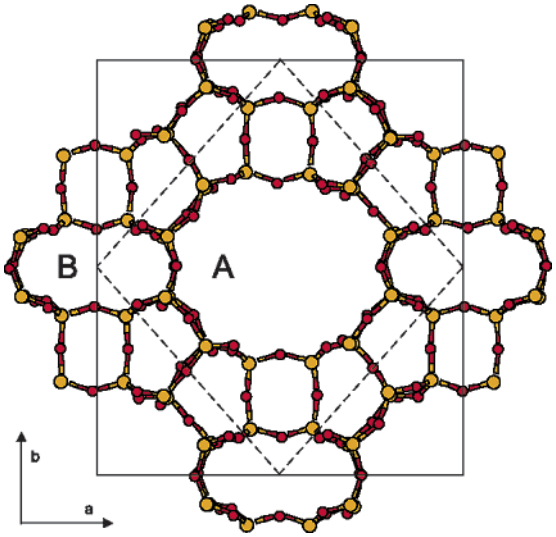

Figure 1. Projection of the mordenite framework along the *c* axis. The largest channels are twelve-membered ring (A) and eight-membered side channel (B). Full (dotted) lines indicate orthorhombic (monoclinic) unit cell.

portant zeolite mordenite. The contact of the extra-framework Al^{3+} with the inner surface of the zeolite leads to a local relaxation and/or reconstruction. At each site, however, the EFAL remains undercoordinated and represents an active center. The strength of active sites originating from extra-framework Al^{3+} is studied through adsorption of CO and confronted with the adsorption at a Na^+ cation, a three-coordinated surface Al-atom, a Brønsted acid site, a surface silanol group, and in purely siliceous zeolites.

2. Scenario for the Formation of Strong Lewis Sites

For the family of mordenite structures, two symmetries are observed. The higher *Cmcm* symmetry is determined for the purely siliceous structure and for low Al mordenites.[18,19] With increasing concentration of framework Al atoms, the number of extra-framework cations also increases, leading to the reduction of symmetry from *Cmcm* to *Pbcn*.[20−23] The structure of mordenite is displayed in Figure 1. The view along the **c** axis shows the main channel (Figure 1, A) circumscribed by 12-membered rings (12MR) of tetrahedral (Si/Al) atoms. The smaller oval channel surrounded by 8MR is referred to as the side pocket (Figure 1, B). The side pocket is accessible from the main channel only along the **b** direction through a 8MR of regular shape. Because the large channels are separated by massive building blocks, the mordenite structure possesses a high thermal stability and a large resistance against acid leaching.

The orthorhombic unit cell contains 144 atoms. The choice of the primitive monoclinic cell (cf. Figure 1), however, decreases the number of atoms to 72. The orthorhombic unit cell of natural mordenite has the lattice parameters $a = 18.09$ Å, $b = 20.52$ Å, and $c = 7.52$ Å.[18] The natural mineral contains a relatively high concentration of framework Al atoms (Si/Al = 4−5). The stability against acid leaching, however, allows a removal of almost all aluminum atoms, thus producing essentially pure-silica mordenite.[24]

The optimization of the cell parameters of the pure-silica mordenite using the generalized gradient approximation (GGA, cf. below), as performed in our previous work,[25] leads to lattice vectors $a = 18.260$ Å, $b = 20.706$ Å, and $c = 7.606$ Å. A slight expansion of the cell, compared with the experimental determinations, reflects underestimation of bonding in GGA and is in line with results reported on other zeolites[6,26−28] and silicates.[29] The structural models presented in this work contain only small number of Si/Al substitutions. The largest substitution rate is 3 Al per cell (Si/Al = 7). All simulations are therefore performed with the unit cell optimized for pure-silica mordenite.[25]

In our previous work[17] we have simulated the dynamical behavior of neutral EFAL particles $Al(OH)_3(H_2O)$ that appear to be more stable in a dehydrated zeolite than hexacoordinated $Al(OH)_3(H_2O)_3$. Our simulation reveals strong basic properties of the neutral hydrated EFAL, leading to frequent proton jumps from the zeolite acid sites to the adsorbed particle. The number of transferred protons depends on the location of the particle and on the concentration of framework Brønsted acid sites. At a high concentration of the acid sites the charge of the EFAL particle due to the proton-transfer varies between +1 and +3. The protonation of EFAL is expressed by eq 1

$$3(AlO_4)_{zeo}{-}H + Al(OH)_3(H_2O) \rightarrow 3[(AlO_4)_{zeo}^{-}] + Al(H_2O)_4^{3+} \quad (1)$$

where $(AlO_4)_{zeo}{-}H$ is the Brønsted acid site of the zeolite and $(AlO_4)_{zeo}^{-}$ is a deprotonized fragment of the framework bearing the negative charge. In water solution, however, the EFAL particle increases the coordination number to six, producing the most stable hydrated form of the Al cation:

$$Al(H_2O)_4^{3+} + 2H_2O \rightarrow Al(H_2O)_6^{3+} \quad (2)$$

When an acid zeolite is immersed in water, small water molecules penetrate into all channels and cavities of the framework. Simulations of acid zeolites loaded with water molecules have shown that a cluster as small as three molecules[30] or even two molecules[31,32] is basic enough to attract the zeolite acid proton and keep it away from the zeolite framework. Brønsted protons in a hydrated zeolite are therefore not localized at the zeolite framework but transferred to intrazeolite water clusters $n(H_2O)_{zeo}$ according to the reaction

$$(AlO_4)_{zeo}{-}H + n(H_2O)_{zeo} \rightarrow (AlO_4)_{zeo}^{-} + n(H_2O){\cdot}H^{+} \quad (3)$$

A more realistic scenario for the proton transfer to a mononuclear EFAL species in a hydrated acid zeolite is therefore

$$3{\cdot}(nH_2O){\cdot}H^{+}_{zeo} + Al(OH)_3(H_2O)_3 \rightarrow (nH_2O)_{zeo} + Al(H_2O)_6^{3+} \quad (4)$$

According to eq 4, in the acid zeolite the EFAL particle collects as many protons from intrazeolite water clusters as necessary to form a stable $Al(H_2O)_6^{3+}$ particle. The charge of any such particle is balanced by three framework Al/Si substitutions. The hexacoordinated $Al(H_2O)_6^{3+}$ adsorbs through hydrogen bonds to the framework O-atoms. The most stable position is near the framework Al-atom(s). In this hydrated form, however, the central atom of the EFAL particle has a fully saturated coordination sphere and does not represent an active center that could play a role in intrazeolite conversions of molecules.

The preparation of zeolite-based catalysts involves drying under vacuum and removing adsorbed molecules, and the catalytic activity finally develops through baking under severe thermal conditions ($T \cong 700$ K). We expect that under such

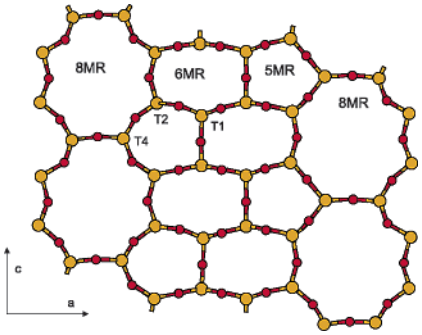

Figure 2. The framework of the main channel of MOR projected into the *ac* plane (cf. Figure 1). Two chains of eight-membered rings (8MR) extended along **c** are interconnected with the network of six- and five-membered rings (6MR and 5MR). T1, T2, and T4 indicate inequivalent tetrahedral positions.

dehydrating conditions the coordination sphere of the EFAL particle is completely destroyed according to the reaction

$$Al(H_2O)_6^{3+} \rightarrow Al^{3+} + 6H_2O \qquad (5)$$

and water molecules are liberated from the zeolite framework, leaving a bare Al^{3+} cation deposited on the inner surface of the zeolite. Relevant intrazeolite processes, such as diffusion of guest molecules, adsorption, molecular interactions leading to a conversion of any kind, are supposed to take place in the largest channels or cavities. In this work we consider Lewis sites produced by the deposition of a single Al^{3+} cation in the main channel of mordenite. One such cation balances the charge of three Al/Si framework substitutions. The corresponding three Al atoms are distributed over the unit cell at large distances to avoid a high local concentration of Al-substituted sites. Of particular importance is the fact that only one Al atom is placed in the main channel representing the only active site accessible to adsorbed molecules. The other two Al atoms are located in the side channel (cf. Figure 1). Figure 2 shows the framework circumscribing the main channel of mordenite composed of 8-, 6- and 5MR's. Due to its small diameter, the Al^{3+} cation can easily pass through the large 8MR and penetrate the structure, thus moving away from the main channel.[33] The accommodation of the cation inside the structure, however, prevents a contact between the EFAL and the adsorbed molecule that is necessary for adsorption and effective interaction. We suppose that EFAL particles nested deep in pores of the zeolite structure play no active role in intrazeolite chemistry. The active centers could be only those cations that are anchored directly at the walls of the main channel. The possibility of an effective immobilization of an Al^{3+} cation is therefore examined for the small 6MR and 5MR (Figure 2).

3. Density-Functional Calculations

Periodic ab initio total energy calculations are performed to fully relax the crystal structure and to localize the extra-framework cation. High-temperature molecular dynamics (MD) simulations are conducted to enable diffusion of the extra-framework cation, the anchoring of the cation at the stable position, and potential local reconstruction. Our DFT-based calculations[34] use the generalized-gradient approximation[35] to the exchange-correlation functional. We use ultrasoft pseudopotentials[36,37] and a plane-wave basis as implemented in the Vienna ab initio simulation package VASP.[38] The calculations are performed using Blöchl's projector augmented wave technique[39,40] with a plane-wave cutoff energy of 400 eV. Due to the large volume of the unit cell, Brillouin-zone sampling is restricted to the Γ-point. Convergence is improved using a modest smearing of the eigenvalues. The optimization of atomic geometries is performed via a conjugate-gradient algorithm with the convergence criterion of 10^{-5} eV. In the relaxation procedure no symmetry restrictions are applied. High-temperature molecular dynamics simulations are performed at 700 K. The molecular dynamics uses the exact Hellmann−Feynman forces acting on atoms and applies the statistics of the canonical ensemble to the motion of atomic nuclei,[41] using the Verlet velocity algorithm[42] with a time step for the integration of equations of motion of $\Delta t = 1$ fs. A simulation time of 1−2 ps is used to check the stability of the location of the extra-framework cation. The stretching frequency of the CO molecule adsorbed at different sites is calculated via the Fourier transform of the velocity autocorrelation function using a MD simulation time of 4 ps. Simulations of the adsorption at sites with the adsorption energy higher than 30 kJ/mol are performed at 100 K. To prevent desorption from weakly attracting sites corresponding MD simulations are performed at 40 K.

4. Results

4.1. Deposition of Al^{3+}. Following the scenario sketched in Section 2 in the periodical structure of mordenite, we consider the existence of the charged EFAL particle that is decomposed to bare Al^{3+} cations (eq 5). We deposit the extra-framework Al^{3+} cation on the inner surface of the main channel. The charge of the extra-framework cation is balanced by three Al/Si substitutions in the zeolite framework, one placed in the main channel and other two located inside the structure. A deposition of the Al^{3+} cation directly in the main channel of mordenite is studied in detail for small windows in the network composed of 5MR, 6MR and 8MR. The framework of the main channel is composed of three different tetrahedral (T) centers (cf. Figure 2 and ref 21). A deposition of the extra-framework Al^{3+} in the vicinity of the zeolite framework is checked for the framework Al atom located in each of the three T centers. Only two inner surface locations of the extra-framework Al atom are observed: in the 6MR and in the 5MR. The 8MR is too large to entrap the small Al^{3+} cation on the surface. Upon penetration into the structure, the Al^{3+} cation loses the character of the surface active site. Extra-framework cations accommodated inside the structure play no active role in catalytic conversions and are therefore in the present work not considered.

EFAL in 6MR. When the framework Al atom resides in position T1 (cf. Figure 2) the deposited Al^{3+} can move either to the 5MR or to the 6MR. Because of the buckling of the zeolite framework, the position T1 is pushed deeper into the structure. For Al in this position, the deposited cation cannot be stabilized in the 5MR and always moves into the 6MR. The shift of the EFAL into the 6MR, however, leads to two different structures. The upward move of the EFAL from the position close to T1, marked in Figure 2, brings it into a relatively symmetrical position within the 6MR (Figure 3a). The move into the second 6MR (right down in Figure 2) places the EFAL into the 6MR with the Al atom in the corner. Both static relaxation of the structure and high-temperature MD simulation show that any location of EFAL in 6MR is unstable and lead to rather progressive local reconstruction of the framework as a consequence of the flexibility of the 6MR. A much better accommodation of the EFAL particle, however, is achieved for the former location that is more symmetrical and ∼90 kJ/mol more stable than the latter location. The final relaxed structures are displayed in Figures 3b and 3c. The extra-framework Al^{3+} cation

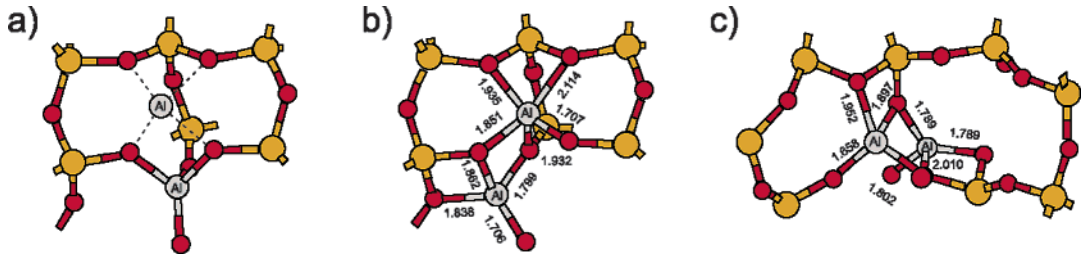

Figure 3. Local relaxations produced upon deposition of extra-framework Al^{3+} cation in the 6MR. The starting point for the relaxation (a). Square-pyramidal coordination of the Al atom formed upon the local relaxation of the framework (b). Quasi-tetrahedral coordination) formed for the Al/Si substitution in the corner of the 6MR (c). Interatomic distances are in angstroms.

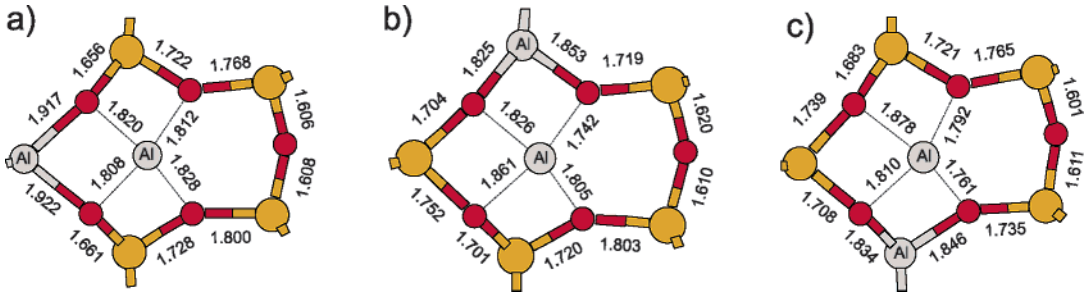

Figure 4. The extra-framework Al^{3+} cation deposited in 5MR. The Al/Si substitution in the position T4 (a) and T2 (b, c).

is incorporated into the framework and becomes part of the structure. The framework Al atom is pushed deeper into the structure and the deposited Al remains at the inner surface of the zeolite. It connects to the framework Al atom via two bridging O atoms. The interatomic distances indicate that the coordination number of the deposited atom is between 4 and 5. Figure 3b displays five Al−O bonds. Note, however, that the length of one of them is with ∼2.1 Å much longer than typical Al−O distances that range, for example, in a defect-free H-zeolite between ∼1.70 and ∼1.85 Å and in corundum from 1.86 to 1.97 Å.[43]

The locally relaxed fraction of the structure composed of two Al atoms and several oxygen atoms formed upon deposition of the extra-framework Al^{3+} cation within the 6MR of mordenite represents an "amorphous" microparticle similar to those observed in Al MAS NMR experiments.[2,3] The formation of the "amorphous" particle, comprising approximately 10 atoms, does not lead to the amorphization of the framework over a large distance and any structural degradation. The particle is located directly at the inner surface of the main channel and is well accessible to molecules adsorbed in the zeolite. The deposited bare Al atom is bound to the structure via the framework oxygens and remains considerably undercoordinated. Such an amorphous particle therefore represents potential active center of the zeolite.

EFAL in 5MR. When the framework Al is located in position T2, the deposited Al^{3+} cation can move to any of three surrounding windows (8MR, 6MR, 5MR; cf. Figure 2). From the position T1 final locations in the 8MR and in the 5MR are possible. The location in the 6MR has been characterized above and the diffusion of Al into the 8MR does not produce a center important from a catalytic point of view. Very promising seems, however, the location of the extra-framework Al^{3+} cation in the 5MR. Both static relaxations and high-temperature MD simulations of the zeolite structure performed at 700 K show that deposition of Al in 5MR is stable. Similar structures are obtained for framework Al atoms located in positions T4 and T2 (Figures 4a−c). No framework reconstruction is observed for deposition of Al in the 5MR. The four framework oxygen atoms making contact with the deposited Al atom are relaxed,

TABLE 1: Energetics of Lewis Sites Formed upon Deposition of the Al^{3+} Cation on the Inner Surface of the Zeolite Framework[a]

	coordination of Al^{3+}	energy
Al^{3+} in 6MR	square-pyramidal (Figure 3b)	0
	quasi-tetrahedral-1 (Figure 3c)	+89
	quasi-tetrahedral-2	+147
Al^{3+} in 5MR	square-planar (Figure 4b)	+222
	square-planar (Figure 4c)	+245
	square-planar (Figure 4a)	+318

[a] Energies in kJ/mol.

deforming the shape of the rather regular 5MR. Despite a considerable Al−O attraction the extra-framework Al^{3+} cation is not placed in the plane of the framework oxygen atoms. It remains in out-of-plane position with the O−Al−O angles 145−160° and unusually long Al−O distances. For tetrahedrally coordinated framework Al atoms, Al−O distances of 1.68 to 1.71 Å are observed.[27] The Al atoms deposited in the 5MR deposited are located at distances of 1.74 to 1.87 Å from the framework O atoms (Figure 4). The larger interatomic distances determined by the out-of-plane position of Al^{3+} and by the limited flexibility of the zeolite framework indicate that the deposited Al atoms are considerably undercoordinated. Moreover, because of the topology of the zeolite framework a specific quasi-planar coordination of Al takes place, leaving the axial directions free for effective interactions. The deposition of the extra-framework cation in the small 5MR of the zeolite structure leads to a trapping of the cation without any reconstruction of the framework. This means, however, that no major stabilization takes place and that the structure with the trapped cation possesses a high energy content. Keeping the other two Al/Si substitutions in the side channel unchanged, the structures displayed in Figures 3 and 4 exhibit rather large differences in energy (Table 1). The most stable location appears to be the reconstructed framework with Al in the 6MR (Figure 3b). Surprisingly large differences are observed for different locations of the framework Al atom. The structure with Al in the position T2 (Figures 4b and 4c) is higher in energy by ∼230 kJ/mol and Al in position T4 (Figure 4a) is ∼320 kJ/mol less stable than the reconstructed zeolite displayed in Figure 3b.

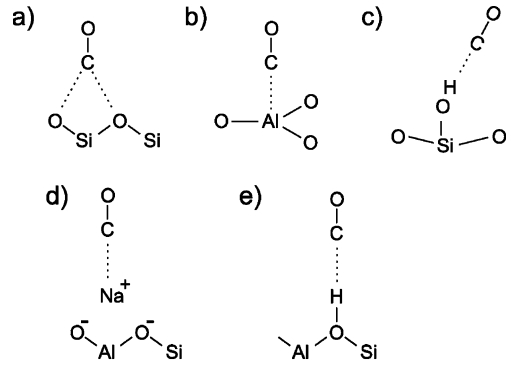

Figure 5. Active sites in the bulk and on the surface of mordenite. Nonspecific adsorption in the pure-silica zeolite (a), and the specific adsorption on the surface three-coordinated framework Al atom (b), surface silanol group (c), extra-framework Na^+ cation (d), and on the Brønsted acid site (e).

Nevertheless, the extra-framework Al atom trapped in the 5MR at the inner surface of the main channel represents a metastable configuration. The conversion to a stable locally reconstructed configuration requires a transfer of the extra-framework ion from the 5MR to some larger ring, 6MR or 8MR. The partial disconnection from the O-atoms of the 5MR, however, represents a barrier to the stabilizing conversion. To inspect the height of the barrier, a series of high-temperature simulations have been performed. Metastable configurations displayed in Figure 4 were equilibrated at 700 K comparable with temperatures of thermal treatment of zeolites. The simulations has shown considerable rigidity of atoms of the 5MR. Because of the limited mobility of the supporting atoms, no one Al^{3+} is shaked-off the small ring. No one transfer to a relaxed structure has therefore been observed, evidencing a high barrier of the transfer and relative stability of the configurations with the Al^{3+} cations trapped in the 5MR. The in-plane oriented bonding of the cation to the supporting oxygen atoms at relatively large distances, however, keeps the cation strongly undercoordinated with axial directions free for interactions with sorbate molecules. Extra-framework Al atoms trapped in small rings of the framework thus could be active sites of extremely high strength.

4.2. Adsorption of CO. The evaluation of the strength of the Lewis sites in mordenite is performed via the adsorption of CO. The CO molecule is a good candidate for such an comparison because a wealth of experimental data exists for mordenite,[44−47] ZSM5,[48,45,46,49] ferrierite,[50] Y[46,51,47,52,49], X,[53,47] and L zeolite,[46] as well as for SiO_2[54] and silica−alumina.[51] Carbon monoxide is known to form adducts through both the C- and the O-atom, depending on the character of bonding to the support. No flat adsorption is observed. For Lewis sites in the zeolite, we compare C- and the O-adsorption. Recently, Bucko et al. reported DFT-simulation of the interaction of CO with different forms of active sites (Brønsted sites, terminal silanols, surface defects) in mordenite.[55] Here we present the comparison of the adsorption energies for the Lewis sites characterized above and compare them with other forms of active sites. Figure 5 displays the structural arrangement upon adsorption of CO at commonly accepted active sites, such as Brønsted acid sites and extra-framework alkali atoms. Surface active sites are represented by silanol groups and by a three-coordinated Al atom and, finally, the adsorption at the pure-silica framework is given for comparison. Table 2 reports calculated adsorption energies and selected geometry parameters and Figure 6 shows the correlation of the adsorption energy and the C−O interatomic distance.

TABLE 2: Calculated Adsorption Energies and Selected Geometry Parameters of CO Adsorbed on Active Sites of Mordenite[a]

	adsorption energy		C−O distance		X−Y distance[b]	
active site[c]	-CO	-OC	-CO	-OC	-CO	-OC
sLS-1	138.7	93.4	1.130	1.159	2.108	1.973
sLS-2	146.0	91.6	1.129	1.160	2.106	1.966
sLS-3	154.3	97.2	1.130	1.161	2.092	1.954
sLS-4	139.0	88.0	1.132	1.159	2.100	1.971
wLS-5	52.8	20.1	1.134	1.148	2.211	2.408
sLS-3[d]	57.5	19.8	1.135	1.146	2.173	2.200
sLS-t	37.7	16.3	1.135	1.145	2.246	2.756
Bas-1	28.6	19.2	1.137	1.145	1.895	1.913
Bas-2[d]	33.5	19.1	1.137	1.145	1.906	1.954
Na-1	28.1	20.4	1.136	1.147	2.595	2.506
Na-2	29.1	22.6	1.135	1.148	2.572	2.487
ss-1[d]	16.3	8.3	1.140	1.144	2.134	2.198
ss-2[d]	17.7	10.1	1.139	1.144	2.149	2.114
nsa-1	7.3		1.142		4.02	
nsa-2	6.7		1.142		3.98	

[a] Adsorption energies in kJ/mol, interatomic distances in angstroms, and angles in degrees. [b] Shortest distance between CO and the zeolite. [c] sLS = strong Lewis site (Figure 4); wLS-5 = weak Lewis site with pentacoordinated extra-framework Al atom (Figure 3b); wLS-3 = site with three-coordinated surface framework Al atom; wLS-t = site with quasi-tetrahedral extra-framework Al atom (Figure 3c); Bas = Brønsted acid site; ss = surface silanol; nsa = nonspecific adsorption. [d] Data for wLS-3, Bas-2, ss-1, and ss-2 are taken from ref 55 to complete the series of zeolite active sites.

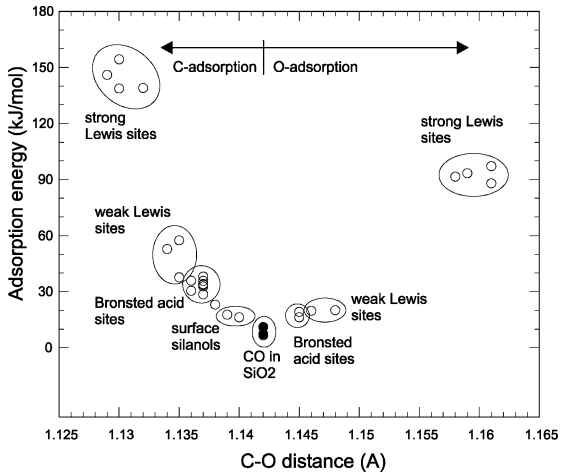

Figure 6. Calculated adsorption energies of CO on different sites in mordenite. Full circles indicate smallest values observed for the pure-silica zeolite. Two branches of the curve are displayed for the C-adsorption (left) and for the O-adsorption (right). Strong Lewis sites are extra-framework Al^{3+} cations trapped in 5MR of the zeolite framework.

The main characteristic of the interaction between CO and the active site of the zeolite is the transfer of electron density from the molecule to the zeolite. Carbon monoxide is a donor and the zeolite an acceptor of electron density.[58] Calculated energies for the adsorption through the C atom are more than ∼50% higher than those for the O-adsorption (Table 2 and Figure 6). A more effective bonding therefore takes place when the "larger and softer" C rather than "smaller and harder" O atom makes contact with the active site. The weaker O-adsorption is observed only at low temperatures. In IR spectra of e.g. H−Y and Na−ZSM-5 a low intensity band red-shifted to 2124 and 2112 cm^{-1}, respectively, is well distinguished below 200 K.[56,57] At room temperature, however, only the C adsorption is of practical importance for the interpretation of experimental data.

Figure 6 and Table 2 show that the active sites of zeolites fall into categories of considerably different adsorption strength. The same order of sites is observed for both C- and O-adsorption. The pure silica structure exhibits the weakest affinity to adsorb CO. The calculated adsorption energy of ~10 kJ/mol is in agreement with a reported experimental value 11.3 kJ/mol.[54] The pure-silica zeolite, in fact, does not contain any localized active sites. Only nonspecific adsorption takes place, and the adsorbed molecule is stabilized through long-range electrostatic interactions. The sorbate−sorbent distance is relatively large but shorter than the radius of the channel. A molecule within the channel is therefore off-centered. In the most stable position, CO does not point to the zeolite surface but extends along the channel with either upward or downward orientation relative to the *c* axis.

Slightly larger stabilization is observed for the adsorption at surface silanol groups. Calculated adsorption energies at several selected O−H groups are 16 to 18 kJ/mol. The larger adsorption energy, compared with the pure-silica zeolite, drives the CO molecule into a localized position. The molecule binds to the H atom at a distance of ~2.10 Å (Table 2), and the orientation is approximately parallel with the O−H bond.

Brønsted acid protons represent active sites with a strength spreading over a relatively large interval of adsorption energies. Table 2 and Figure 6 comprise Brønsted sites both in the bulk and at the surface of mordenite. From the large number of possible locations, bulk sites localized in the main channel and sites on the 001 surface[59] have been selected. For weaker Brønsted acid sites in the bulk, the adsorption energy is comparable with that of stronger surface Brønsted sites. The largest observed adsorption energies for Brønsted acid sites of ~30−40 kJ/mol are comparable with the adsorption energy of the weakest Lewis site (cf. Table 2 and Figure 6). Sites with considerably different strength exist both in the bulk and on the surface. No clear correlation, however, is observed between the location of the site and its adsorption strength.

Higher adsorption energies than for Brønsted acid sites are observed for Lewis sites. Two values listed in Table 2 are obtained for Al deposited in the 6MR (one such configuration is shown in Figure 3b) and for three-coordinated surface Al-atom. The energies span a relatively large interval from ~38 to ~58 kJ/mol. The smallest value of ~38 kJ/mol is obtained for a reconstructed configuration with the extra-framework Al deposited in the 6MR and relaxed to a quasi-tetrahedral coordination. As a consequence of the high degree of accommodation, the bonding capacity of the Al atom to form another bond decreases and the adsorption energy is relatively small. Note that the calculated adsorption energy of such a cation is lower than energies of strongest Brønsted acid sites. A much higher energy of ~53 kJ/mol is obtained for similar cation that is, however, relaxed to form a quasi pentacoordinated surface Al atom at the inner surface of the main channel (Figure 3b). In this configuration Al is uncoordinated in the direction perpendicular to the surface, and this allows a stronger interaction with the adsorbed molecule than for a quasi-tetrahedral Al. The highest adsorption energy of ~58 kJ/mol is obtained for a three-coordinated framework Al atom at the surface.[55] In our previous work we reported that such an active surface atom is formed upon dehydration of the zeolite surface,[59] and recently van Bokhoven et al. showed by XANES experiments that the concentration of the three-coordinated Al atoms is a function of temperature and pretreatment of the zeolite.[60] The planar bonding of the Al atom with three framework O-atoms leaves two perpendicular directions unoccupied. The calculated energies reported in Figure 6 and Table 2 demonstrate that such under-coordinated surface Al atoms are almost twice-as strong adsorption centers than Brønsted acid sites. In Figure 6 yet another surface site is displayed between Brønsted sites and surface silanols. This is the Brønsted acid site located directly at the 2MR formed upon dehydration of the zeolite surface.[59] The calculated energy of ~23 kJ/mol shows that strength of such a site is relatively low.

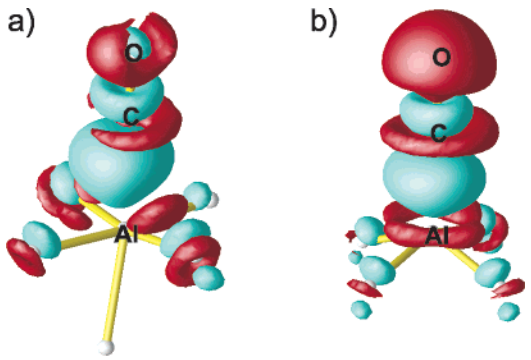

Figure 7. Difference electron densities of CO adsorbed at weak (a) and strong (b) Lewis sites. For the atomic configurations see Figures 3b and 4b. Light gray regions indicate a gain and the dark regions a depletion of the electron density (same isosurfaces apply for both figures).

The extra-framework Al cations trapped in the 5MR of the zeolite framework are in Figure 6 denoted as strong Lewis sites. Figure 4 shows that for Al^{3+} cations in the 5MR of mordenite a relaxation, but no reconstruction, of the framework occurs. In the quasi-planar tetra-coordination of Al (Figure 4) optimal Al−O separations are not achieved because of the local limited flexibility of the framework. Due to the combination of two phenomena, the undercoordination in the equatorial plane and the two unoccupied axial positions, the extra-framework cation is an extremely strong adsorption center. The adsorption energies in Figure 6 and Table 2 show that strong Lewis sites are approximately three times stronger than weak Lewis sites.

For the extra-framework cation in the 5MR, three locations of the framework Al have been examined (Figure 4) with the framework Al atom in T2 and T4 (Figure 2). Preliminary calculations indicate that Al in positions T2 and T4 stabilizes the extra-framework Al^{3+} stronger compared with the position T1 (Figure 2). For the configuration displayed in Figure 4a, however, pronounced local deformation is observed. This instability is caused by the close proximity of the second framework Al atoms located in the same 4MR (not displayed in Figure 4a). At high temperatures such a local concentration of Al atoms leads to a reconstruction of a local character similar to that caused by an extra-framework Al atom deposited in the 6MR (cf. Paragraph 4.1 above and Figure 3b). Better thermal stability is observed for a configuration with framework Al atoms placed at larger distance in the framework. The fourth inspected configuration possesses the same local geometry as displayed in Figure 4a, but differs in the position of the second framework Al atom (not displayed). This configuration is stable at high temperatures.

All the Al ions in the 5MR exhibit similar adsorption energies (Figure 6). The five-membered rings of the zeolite structures thus seem to act as traps for small cations such as Al^{3+}, leading to the formation of strong Lewis sites.

Figure 7 compares bonding at weak and strong Lewis site. The difference electron density is calculated as the difference in the electron density of CO adsorbed on the Lewis site, and of a free CO molecule and the atoms forming the active site,

TABLE 3: Calculated Stretching Frequencies of CO and Averaged Geometry Parameters of CO Adsorbed on Active Sites of Mordenite as Resulting from MD Simulation[a]

	C-adsorption					O-adsorption				
active site[b]	f	Δf	C−O	C−X[c]	O−C−X	f	Δf	CO	C−X[c]	O−C−X
sLS-1	2244	116	1.127	2.123	172.9	1951	−177	1.163	1.982	167.0
sLS-4	2227	99	1.127	2.128	173.2	1975	−153	1.160	2.000	167.9
wLS-5	2193	65	1.133	2.240	167.6	2071	−57	1.147	2.527	167.4
sLS-3	2188	69	1.133	2.194	172.2	2087	−41	1.145	2.241	171.6
Bas-1	2170	42	1.137	1.981	165.5	2092	−36	1.144	2.076	169.2
Bas-2	2164	36	1.136	1.954	169.6	2092	−36	1.143	2.054	166.2
Bas-2[e]	2178	50				2106	−22			
Na-1	2155	27	1.136	2.686	166.9					
Na-2	2155	27	1.137	2.702	162.7					
ss-1	2146	18	1.138	2.169	173.5					
ss-2	2138	18	1.138	2.126	172.6					
CO in SiO_2	2128	0	1.142	1.981	108.2					
in vacuo	2128[d]	0	1.142							

[a] Adsorption energies in kJ/mol, interatomic distances in angstroms, and angles in degrees. [b] Notation as in Table 2. [c] Shortest distance between CO and the active center of the zeolite. [d] Frequency calculated as the average of P and R branches located at 2103 and 2152 cm^{-1}. [e] Harmonic approximation (ref 55).

both deformed to their respective geometry in the adsorption complex. Such a difference in electron density shows the change of the electron density distribution induced by the adsorption. Changes are observed within the adsorbed molecule and in the vicinity of the Al atom and of the framework O atoms, respectively. The electron density around the oxygen atom of the adsorbed molecule is attracted toward the atomic nucleus, thus shrinking the size of the ion. On the C atom the nonbonding electron density is clearly depleted and transferred into the C−O bond on one side and into the region between the Al atom and the molecule on the other side. The region adjacent to the Al atom is slightly electron depleted. The electron density on the framework O atoms shows a polarization similar to that of the C atom. The nonbonding electron density is depleted and stretched in both directions along the O−Al and O−Si bonds, respectively. The pattern of the rearrangement of the electron density is qualitatively the same for both weak and strong Lewis sites, but the depletion of the O-end of the adsorbed molecule and of the region between Al and C is more pronounced for strong Lewis sites. This means that despite the huge difference in the strength of both sites the same bonding mechanism applies when the CO molecule is adsorbed. On the strong Lewis site, however, all observed changes are more pronounced.

4.3. Stretching Frequencies of CO. IR spectroscopy of the adsorbed CO is a powerful tool routinely used to characterize the strength of active sites in zeolites. For adsorption at the Lewis sites described above, we perform molecular dynamics simulations to reproduce the IR spectral bands. The CO stretching frequencies are obtained through Fourier transform of the atomic-velocity autocorrelation function. The geometry parameters, such as the CO interatomic distance and the distance of the molecule from the zeolite active center, are averaged over all configurations of the MD run each consisting of 4000 steps. In Figure 8 the calculated stretching frequencies of CO adsorbed on Lewis sites are displayed together with those simulated for other types of active sites (Figure 5). Corresponding frequencies and geometry parameters are collected in Table 3. Note that MD-averaged parameters (Table 3) agree well with those from static relaxation of the structure (Table 2). Figure 8 shows that the correlation between the CO stretching frequencies and the CO distance is linear. The linearity holds for all active sites and for both types of the adsorption, stronger C-adsorption and weaker O-adsorption. The stretching frequency of 2128 cm^{-1} calculated for the free gas-phase molecule also fits the dependence (filled circle in Figure 8). This frequency agrees reasonably well with the experimental value of 2140 cm^{-1}.[61] Both the calculated and experimental frequencies are the averaged value of two rotational−vibration (P and R) branches of the diatomic molecule. Figure 8 shows that red-shifted frequencies, i.e., frequencies lower than that of the nonadsorbed molecule, are obtained for the molecules adsorbed via the O-atom. As already mentioned above, in zeolites this type of adsorption is only of marginal importance, because of the far smaller adsorption energies compared to adsorption via the C-atom (cf. Table 2 and Figure 6). For the CO molecule adsorbed in the pure-silica zeolite, the same frequency of 2128 cm^{-1} is calculated as for a molecule in vacuo. This means that long-range electrostatic interactions between the framework and the molecule have no influence on the stretching frequency of the adsorbed molecule. The same frequency of 2140 cm^{-1} as for gaseous CO is observed for CO weakly physisorbed CO SiO_2 surfaces, as well.[54] The comparison of measured and calculated frequencies of nonadsorbed molecules and molecules adsorbed in pure-silica zeolites indicates that a systematic shift of calculated values by some 12 to higher frequencies should be considered.

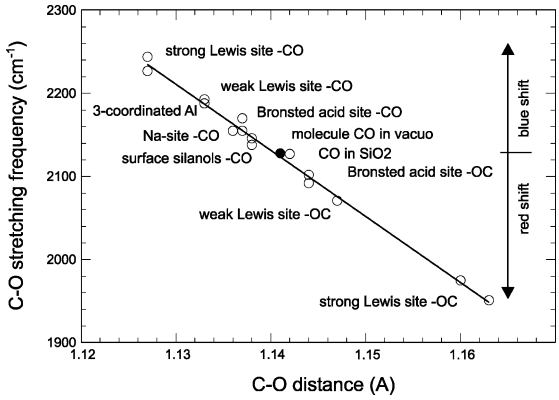

Figure 8. Calculated stretching frequencies of CO adsorbed on different active sites of mordenite. Full circle indicates molecule in vacuo separating blue-shifted (upper) and red-shifted (lower) frequencies.

Figure 9 displays calculated shifts of stretching frequencies of the C-adsorbed molecule relative to free CO along with available experimental data. IR spectra of H-mordenite exhibit three CO stretching bands.[44] In Figure 9 the limits of measured IR bands are sketched as full vertical lines and dashed lines indicate band maxima. The smallest shifts are observed for

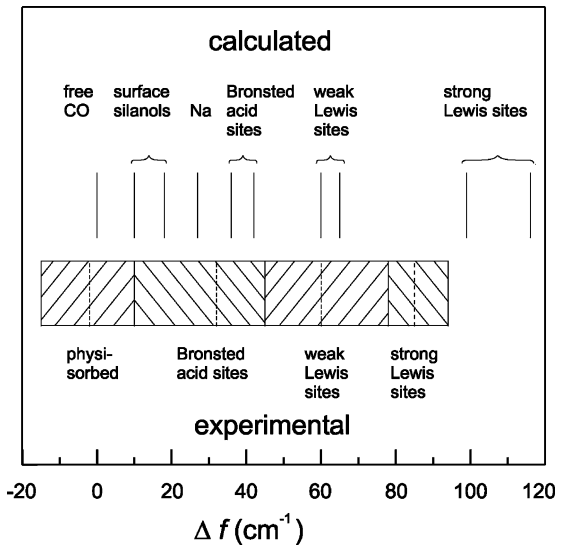

Figure 9. Comparison of shifts of stretching frequencies of CO adsorbed in mordenite relative to free molecule. Experimental frequencies are sketched according to Figure 2 in ref 44. Vertical lines indicate limits of IR bands and dashed lines show band maxima. Calculated frequencies display MD simulated data (cf. Table 3).

weakly physisorbed molecules, and the other two bands are assigned to adsorption at the Brønsted acid sites, and at strong Lewis sites, respectively.[44,51] The measured band maximum of less perturbed frequencies compares well with experimental frequency of free CO. Approximately one-half of the band, however, is downshifted compared with the frequency of free CO. Because a red shift is observed only for O-adsorption (Figure 8), this downshift indicates that a certain fraction of CO physisorbed in the zeolite makes contact to the framework through the O-end, as well.

The small shifts of 10 and 18 cm^{-1} calculated for adsorption at surface silanols agree nicely with the shift of 18 cm^{-1} reported for adsorption on SiO_2 surfaces.[54] In mordenite these frequencies contribute to the lower part of the most intense band spanning a relatively broad interval from 10 to 45 cm^{-1}. The shifts of 36 and 42 cm^{-1} calculated for two Brønsted acid sites agree well with the location of the most intense band, in agreement with traditional interpretation of IR spectra. The band maximum is centered at 32 cm^{-1} in mordenite,[44] at 39 cm^{-1} in Y,[51] and at 31 cm^{-1} in ferrierite.[50] For the adsorption on extra-framework Na^+ cations, we calculate a frequency shift of 27 cm^{-1}, indicating that adsorption on Na^+ produces low-frequency components of the same band as adsorption on Brønsted acid sites. Similar shifts of frequencies for adsorption at Na^+ in both MOR and ZSM5 have been observed in IR spectra.[45]

High-frequency components of the CO stretching shifted by ~85 cm^{-1} are observed in both mordenite[44] and Y zeolite.[51] Less pronounced, but clearly visible are also components centered at ~60 cm^{-1}. These spectral features appear immediately after CO dosage.[51] This is in agreement with our calculated adsorption energies showing large differences between strong Lewis sites (~130−150 kJ/mol), weak Lewis sites (~40−60 kJ/mol), and Brønsted acid sites (~30−40 kJ/mol). Despite the much higher concentration of Brønsted acid sites, adsorbate molecules are attracted first to the strong Lewis sites. Our calculations indicate a frequency shift of ~60 cm^{-1} for weak and of ~110 for strong Lewis sites (Table 3 and Figure 9). While the value calculated for weak site compares well with the observed IR band, the shift calculated for strong Lewis site is considerably exaggerated. The reason is a too strong attraction of the molecule to the adsorption center.

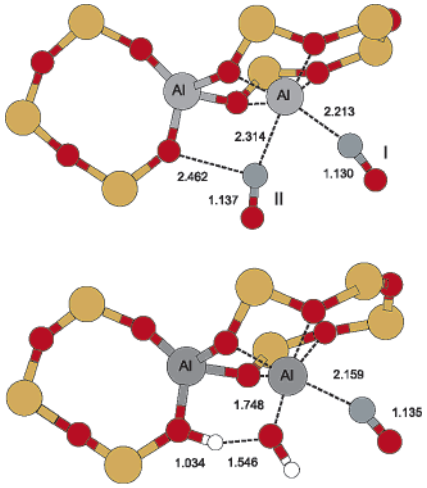

Figure 10. Two CO molecules adsorbed on strong Lewis site in mordenite (top) and simultaneous adsorption of H_2O and CO (bottom). Note the different bonding of two CO molecules. The H_2O molecule on Al^{3+} dissociates producing a Brønsted acid site on the framework and a hydroxyl group connected to the cation.

4.4. Two CO Molecules Coadsorbed at a Strong Lewis Site. The diameter of the Al^{3+} cation trapped in the 5MR of the zeolite (Figure 4) is too large to be accommodated directly in the plane of the 5MR. Thus the cation remains side-connected with an O−Al−O angle of ~150°. In such a position it is strongly undercoordinated and has the capacity to adsorb more than one molecule. A configuration with two molecules adsorbed at an extra-framework Al^{3+} cation is displayed in Figure 10 (top) and compared with a coadsorption configuration of CO and H_2O (bottom). Both molecules are adsorbed via the C-atom, and the calculated adsorption energy is ~154 kJ/mol. The comparison with the adsorption energy of the single molecule (Table 2) shows that adsorption of two molecules on the same center is possible. Bonding of any of two molecules, however, is weaker than that of the single molecule. In the case of equivalent bonding of both molecules the adsorption energy per molecule is ~77 kJ/mol, larger than for the adsorption of a single molecule at a weak Lewis sites (~38 to ~58 kJ/mol; Table 2). Distances of the adsorbed molecules from Al^{3+} (2.213 Å and 2.314 Å, see Figure 10) indicate considerable differences in bonding of the two molecules. Stronger connection is observed for molecule I (Figure 10, top), causing a remarkable contraction of the C−O distance to 1.130 Å. The repulsion between two adsorbed CO molecules keeps molecule II at a slightly larger distance of 2.314 Å. The bond length of this molecule is only moderately reduced to 1.137 Å. Note that for this molecule a contact with a framework O-atom is possible. The CO stretching frequencies of two CO adsorbed at the same Al^{3+} are displayed in Figure 12.

Both frequencies fit the correlation with the CO bond length obtained for a series of different active sites and displayed in Figure 8. The frequency of more strongly bonded molecule I is considerably decreased compared with that of a single adsorbed molecule to 2206 cm^{-1}. Despite the reduction, however, it is still higher by ~20 cm^{-1} than the frequency obtained for a weak Lewis site. The shift relative to a free CO molecule of ~80 cm^{-1} is in reasonable agreement with spectral observations of ~85 cm^{-1} (cf. refs 44,51 and Figure 9). The highest CO stretching frequencies observed in the IR spectra of CO-loaded

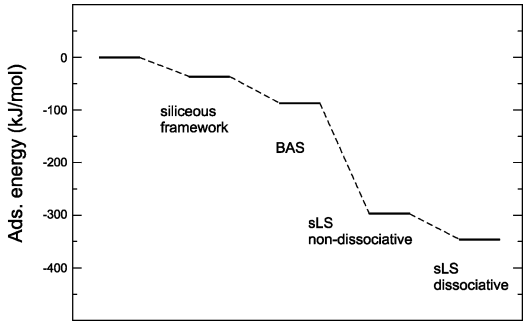

Figure 11. Adsorption energy of H_2O on the siliceous framework, Brønsted acid site (BAS) and strong Lewis site (sLS) in mordenite.

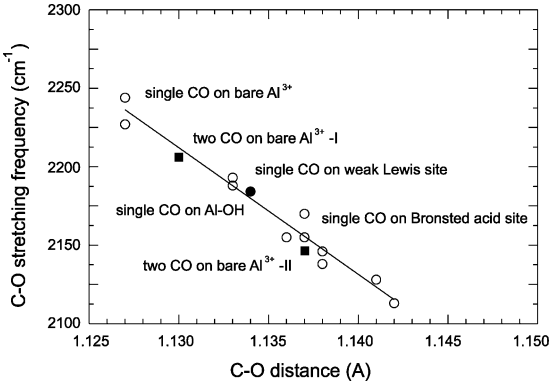

Figure 12. Calculated stretching frequencies of two molecules adsorbed at the strong Lewis site in mordenite. For comparison, empty circles and the straight line display the stretching frequencies of CO adsorbed at different active sites and the correlation with the CO bond length, taken from Figure 8. Filled squares represent two CO on strong Lewis site (Figure 10, top). Filled circle is CO on $Al^{3+}\cdot H_2O$ (Figure 10, bottom).

zeolites are thus assigned to molecules tightly adsorbed at a strong Lewis site. The frequency of the more weakly bound molecule II is only 2143 cm^{-1}, but still blue-shifted. The shift is similar to that for the adsorption at surface silanols. The stretching frequencies of CO weakly bonded to strong Lewis sites thus merge with the broad band comprising Brønsted acid sites and surface silanols and therefore cannot be distinguished in the IR spectrum.

4.5. Hydrated Extra-framework Al^{3+}. The charge of each extra-framework Al^{3+} cation is compensated by three Al/Si framework substitutions. The formation of such a complex of one extra-framework and three framework Al atoms would be supported by a high local concentration of the framework Al/Si substitutions. The substitution in neighboring tetrahedral positions, however, is unfavorable according to Löwenstein's rule. Moreover, controlled Al/Si framework substitutions have shown that in low-Al zeolite two framework Al atoms are never located in the same small ring, such as the 5MR.[62] An extra-framework Al^{3+} cation attached on the inner surface of the zeolite compensate charges of three Al/Si substitutions located in the framework at relatively large distances. The formation of an Al^{3+} cation deposited on the inner surface of the zeolite is therefore energetically very demanding, as already documented by Table 1, because of the large distances between the compensating charges. One can therefore argue that the existence of a bare trivalent extra-framework cation is not possible and that the extra-framework ion can exist only in partially hydrated form. A monohydrated extra-framework Al^{3+} is displayed in Figure 10 (bottom). On adsorption at the Al^{3+} cation, the H_2O molecule dissociates, forming a Brønsted acid site and a hydroxylaluminum cation linked by a hydrogen bond, as already observed by Bhering et al.[5] Such a dissociation considerably reduces the separation of charges and produces an Al−OH particle of increased stability compared with a bare Al^{3+}. The hydroxylaluminum cation has the formal charge 2+ and the extra-framework Al atom is still charge-depleted. Figure 11 compares adsorption energies of H_2O on different sites of the mordenite structure. Adsorption energy on the siliceous framework is ∼40 kJ/mol and on a Brønsted acid site ∼80 to 90 kJ/mol.[63] A huge stabilization of ∼300 kJ/mol is observed upon adsorption on the strong Lewis site. A dissociation produces the Brønsted site and the $Al(OH)^{2+}$ cation that are by ∼50 kJ/mol more stable than nondissociated adsorbed molecule. The calculated adsorption energy of CO on $Al(OH)^{2+}$ (Figure 10, bottom) is only ∼10 kJ/mol. Such a small adsorption energy indicates that hydration of the Lewis center leads to almost complete saturation of the active site. In Figure 12 the adsorption capacity of the hydroxylaluminum cation is compared with that of other active sites. The calculated frequency shift of CO shows that the hydroxylaluminum cation is a stronger acid than a Brønsted site, but weaker than weak Lewis sites and considerably weaker than bare Al^{3+} cations. The shift relative to the free CO molecule is only 56 cm^{-1}. The hydration of the cation thus considerably decreases the adsorption strength of the extra-framework particle. The band of CO stretching modes with frequencies of ∼2230 cm^{-1},[44,51] blue-shifted by ∼85 cm^{-1}, therefore cannot originate from the hydrated extra-framework species. The band at ∼2230 cm^{-1} reflects the presence of bare Al^{3+} cations trapped in small windows of the zeolite framework.

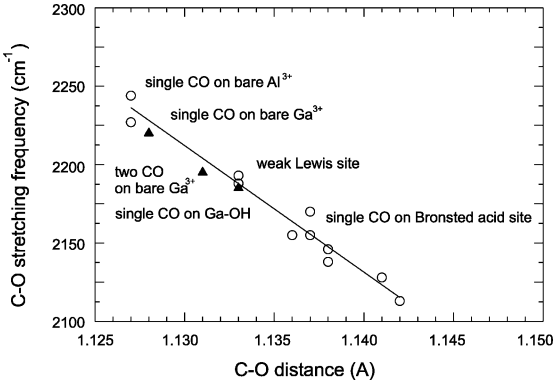

Figure 13. Calculated stretching frequencies of CO adsorbed on Ga^{3+} in mordenite. Empty symbols obtained for other active sites (Figure 8) are displayed for comparison.

4.6. Comparison of Al^{3+} vs Ga^{3+}. The transfer of a hydrated Al^{3+} cation from the solution into the zeolite framework is hindered by large electrostatic barriers. A less polarizing Ga^{3+} cation, however, can be transferred to ion-exchange positions of the zeolite. The direct exchange of a hydrated Ga^{3+} ion is a matter of debate. Instead, solid-state ion exchange is used as a relatively simple procedure.[64−67] Ga-exchanged zeolites are known to be active in numerous catalytic conversions.[64] Experimental probing of the strength of active sites via the adsorption of CO shows for Ga−ZSM-5 an intense band at 2210 cm^{-1},[68] demonstrating a high concentration of strong Lewis sites. The frequency shift of 82 cm^{-1} relative to free CO molecule indicates that the strength of Ga^{3+} is only slightly weaker than that of strongest sites observed in zeolites not containing any exchanged extra-framework cations (85 cm^{-1} [44,51]) and assigned to EFAL particles.

The calculated stretching frequencies of CO adsorbed in Ga-exchanged mordenite are displayed in Figure 13. The same configurations as for the extra-framework Al atom (Figure 10)

are explored. The calculated frequencies of CO adsorbed on Ga (Figure 13) show remarkable similarities with those for adsorption on Al (Figure 12). The stretching frequency of 2220 cm^{-1} of CO adsorbed at a bare Ga^{3+} cation is only slightly lower than 2227 cm^{-1} calculated for Al^{3+} (Table 3). Upon adsorption of a second CO molecule, the frequency is reduced to 2195 cm^{-1} (cf. 2206 cm^{-1} for Al^{3+}, Figure 12). Such a frequency is blue-shifted by 67 cm^{-1}. The good agreement with the intense band in the IR spectrum of Ga−ZSM-5,[68] blue-shifted by 70 cm^{-1}, proves that cooperatively unsaturated extra-framework Ga atoms exist in the form of a bare Ga^{3+} cation trapped on the inner surface of the zeolite. For adsorption on a hydrated extra-framework Ga, a CO stretching frequency 2185 cm^{-1} is calculated, comparable with the 2184 cm^{-1} obtained for the extra-framework Al−OH.

Although the existence of bare Ga^{3+} extra-framework cations is generally accepted, the concept of bare nonhydrated Al^{3+} cations is largely considered to be unrealistic. The exchange of Al^{3+} into the ion-exchange extra-framework position, however, is as impossible as the exchange out of the zeolite framework. Under drastic thermal conditions, routinely used to prepare active zeolites, Al ions are released from the structure and trapped on the inner surface of the zeolite. Most of the cations are stabilized through local relaxation of the structure and only a small fraction of them is trapped in the small windows of the framework producing strong Lewis sites. The concentration of such active centers could be extremely small. However, due to their high adsorption strength and catalytic activity, the strong Lewis site makes a nonnegligible contribution to the catalytic performance of the zeolite. Kazansky et al.[69] have shown that with increasing temperature of dehydration of HZSM-5 (∼700K to ∼900K) a proportional increase of the intensity of the CO stretching band at 2224 cm^{-1} is observed. Our simulation demonstrates that experimentally observed IR bands situated at frequencies above 2200 cm^{-1} correspond to CO adsorbed at bare cations (Al^{3+}, Ga^{3+}). A minimum degree of hydration reduces the adsorption strength of the cation, leading to considerable decrease of the CO stretching frequency.

5. Summary

Our analysis shows that the presence of a strongly blue-shifted component in the CO stretching frequencies of CO-loaded mordenite indicates the presence of strong Lewis sites. In the absence of other exchanged multivalent cations, these strong Lewis sites can be only Al^{3+} ions produced by the dehydration of hydrated form of extra-framework Al particles and anchored in the small rings of the zeolite framework. The existence of the Al^{3+} ions in zeolites goes against some traditionally accepted notions in zeolite science, but our ab initio MD simulations demonstrate that the Al^{3+} cations bound in the 5MR and 6MR's of the mordenite framework are at least metastable at temperatures up to 700 K. The Al^{3+} cations strongly adsorb CO and produce a blue-shift of the CO stretching frequency as large as 100−120 cm^{-1}, i.e., larger as the high-frequency component in the IR spectra. We have shown that the strength of the Al^{3+} Lewis sites is large enough to simultaneously bind two molecules: for two coadsorbed CO molecules, the calculated blue-shift agrees nicely with experiment. However, the dissociative adsorption of a water molecule leads to the formation of an $(Al-OH)^{2+}$ particle of a considerably reduced adsorption strength. Nevertheless, our study demonstrates the presence of strong Lewis acidity in zeolites even if no ion-exchange has taken place.

Acknowledgment. Groupement de Recherche Européen "Dynamique Moléculaire Quantique Appliquée à la Catalyse", founded by the Council National de la Recherche Scientifique (France), the Institut Français du Pétrole (IFP), and the Universität Wien. Facilities at Computing Center of Vienna University (Schrödinger cluster) are kindly acknowledged.

References and Notes

(1) Gola, A.; Rebours, B.; Milazzo, E.; Lynch, J.; Benazzi, E.; Lacombe, S.; Delevoye, L.; Fernandez, C. *Micropor. Mesopor. Mater.* **2000**, *40*, 73.
(2) Omegna, A.; van Bokhoven, J. A.; Prins, R. *J. Phys. Chem. B* **2003**, *107*, 8854.
(3) Omegna, A.; Haouas, M.; Kogelbauer, A.; Prins, R. *Micropor. Mesopor. Mater.* **2001**, *46*, 177.
(4) Arribas, M. A.; Martínez, A. *Appl. Catal. A: Gen.* **2000**, *230*, 203.
(5) Bhering, D. L.; Ramırez-Solís, A.; Mota, C. J. A. *J. Phys. Chem. B* **2003**, *107*, 4342.
(6) Durà-Vilà, V.; Gale, J. D. *J. Chem. Phys.* **2001**, *105*, 6158.
(7) Nachtigallova, D.; Nachtigall, P.; Sierka, M.; Sauer, J. *Phys. Chem. Chem. Phys.* **1999**, *1*, 2019.
(8) Sauer, J.; Nachtigallova, D.; Nachtigall, P. In *Catalysis by Unique Metal Ion Structures in Solid Matrixes. From Science to Application*; Centi, G.; Wichterlova, B., Bell, A. T., Eds.; Kluwer Academic: Dodrecht, 2001; Vol. 13, p 221.
(9) Berthomieuv, D.; Krishnamurty, S.; Coq, B.; Delahay, G.; Goursot, A. *J. Phys. Chem. B.* **2001**, *105*, 1149.
(10) Goursot, A.; Coq, B.; Fajula, F. *J. Catal.* **2003**, *216*, 324.
(11) Barbosa, L. A. M. M.; van Santen, R. A. *Catal. Lett.* **1999**, *63*, 97.
(12) Barbosa, L. A. M. M.; van Santen, R. A.; Hafner, J. *J. Am. Chem. Soc.* **2001**, *123*, 4530.
(13) Barbosa, L. A. M. M.; van Santen, R. A. *J. Mol. Catal. A: Chemical* **2001**, *155*, 101.
(14) Shubin, A. A.; Zhidomirov, G. M.; Yakovlev, A. L.; van Santen, R. A. *J. Phys. Chem. B* **2001**, *105*, 4928.
(15) Barbosa, L. A. M. M.; Zhidomirov, G. M.; van Santen, R. A. Catal. Lett. **2001**, *77*, 55.
(16) Barbosa, L. A. M. M.; van Santen, R. A. *J. Phys. Chem. B* **2003**, *107*, 4532.
(17) Benco, L.; Demuth, T.; Hafner, J.; Hutschka, F.; Toulhoat, H. *J. Catal.* **2002**, *209*, 480.
(18) Alberti, A.; Davoli, P.; Vezzalini, G. *Z. Kristallogr.* **1986**, *175*, 249.
(19) Meier, W. M. *Z. Krislallogr.* **1961**, *115*, 439.
(20) Mortier, W. L.; Pluth, J. J.; Smith, J. V. *Natural Zeolites. Occurrence, Properties, Use*; Pergamon Press: Elmsford, 1978, 1978.
(21) Schlenker, J. L.; Pluth, J. J.; Smith, J. V. *Mater. Res. Bull.* **1979**, *14*, 751.
(22) Schlenker, J. L.; Pluth, J. J.; Smith, J. V. *Mater. Res. Bull.* **1978**, *13*, 169.
(23) Baerlocher, C.; Meier, W. M.; Olson, D. H. *Atlas of Zeolite Framework Types*; Elsevier: Amsterdam, 2001.
(24) Minachev, V.; Garamin, V.; Isakova, T.; Kharamov, V.; Bogondo, V. V. *Adv. Chem.* **1977**, *102*, 441.
(25) Demuth, T.; Hafner, J.; Benco, L.; Toulhoat, H. *J. Phys. Chem. B* **2000**, *104*, 4593.
(26) Rozanska, X.; Demuth, T.; Hutschka, F.; Hafner, J. van Santen, R. A. *J. Phys. Chem. B* **2000**, *106*, 3248.
(27) Benco, L.; Demuth, T.; Hafner, J.; Hutschka, F. *J. Chem. Phys.* **1999**, *111*, 7537.
(28) Benco, L.; Demuth, T.; Hafner, J.; Hutschka, F.; Toulhoat, H. *J. Chem. Phys.* **2001**, *114*, 6327.
(29) Demuth, T.; Jeanvoine, Y.; Hafner, J.; Angyan, J. G. *J. Phys.: Condens. Matter.* **1999**, *11*, 3833.
(30) Termath, V.; Haase, F.; Sauer, J.; Hutter, J.; Parinello, M. *J. Am. Chem. Soc.* **1998**, *120*, 8512.
(31) Nusterer, E.; Blöchl, P. E.; Schwarz, K. *Chem. Phys. Lett.* **1996**, *253*, 448.
(32) Jeanvoine, Y.; Angyan, J. G.; Kresse, G.; Hafner, J. *J. Phys. Chem. B* **1998**, *102*, 7307.
(33) Benco, L.; Bucko, T.; Demuth, T.; Hafner, J., unpublished results.
(34) Jones, R. O.; Gunnarsson, O. *Rev. Mod. Phys.* **1989**, *61*, 689.
(35) Perdew, J. P.; Chevary, A.; Vosko, S. H.; Jackson, K. A.; Pedersen, M. R.; Singh, D. J.; Fiolhais, C. *Phys. Rev. B* **1992**, *46*, 6671.
(36) Vanderbilt, D. *Phys. Rev. B* **1990**, *41*, 7892.
(37) Kresse, G.; Hafner, J. *J. Phys. Cond. Matter* **1994**, *6*, 8245.
(38) Kresse, G.; Furthmüller, J. *Phys. Rev. B* **1996**, *54*, 11169.
(39) Blöchl, P. E. *Phys. Rev. B* **1994**, *50*, 17953.
(40) Kresse, G.; Joubert, D. *Phys. Rev. B* **1999**, *59*, 1758.
(41) Nosé, S. *J. Chem. Phys.* **1984**, *81*, 511.

(42) Allen, M. P.; Tildesley, D. J. Computer simulations of liquids; Clarendon: Oxford, 1987.
(43) Smyth, J. R.; Bish, D. L. *Crystal Structures and Cation Sites of the Rock-Forming Minarals*; Allen & Unwin: Boston, 1988.
(44) Bordiga, S.; Lamberti, C.; Geobaldo, F.; Zecchina, A. *Langmuir* **1995**, *11*, 527.
(45) Lamberti, C.; Bordiga, S.; Geobaldo, F.; Zecchina, A.; Otero Areán, C. *J. Chem. Phys*. **1995**, *103*, 3158.
(46) Borovkov, V. Y.; Jiang, M.; Fu, Y. *Phys. Chem. B* **1999**, *103*, 5010.
(47) Rakic, V.; Dondur, V.; Hercigonja, R. J. *Serb. Chem. Soc*. **2003**, *68*, 409.
(48) Bordiga, S.; Scarano, D.; Spoto, G.; Zecchina, A. *Vib. Spectrosc*. **1993**, *5*, 69.
(49) Otero Areán, C.; Palomino, G. T.; Zecchina, A.; Spoto, G.; Bordiga, S.; Roy, P. *Phys. Chem. Chem. Phys.* **1999**, *1*, 4139.
(50) Bordiga, S.; Palomino, G. T.; Pazè, C.; Zecchina, A. *Micropor. Mesopor. Mater*. **2000**, *34*, 67.
(51) Cairon, O.; Chevreau, T.; Lavalley, J-. C. *J. Chem. Soc., Faraday Trans.* **1998**, *94*, 3039.
(52) Garrone, E.; Bonelli, B.; Tsyganenko, A. A.; Delgado, M. R.; Palomino, G. T. *J. Phys. Chem. B* **2003**, *107*, 2537.
(53) Rudakova, A. V.; Lobo, R. F.; Bulanin, K. M. *J. Phys. Chem. B* **2003**, *107*, 5212.
(54) Beebe, T. P.; Gelin, P.; Yates, J. T., Jr. *Surf. Sci.* **1984**, *148*, 526.
(55) Bucko, T.; Benco, L.; Hafner, J. *J. Phys. Chem. B*, submitted.
(56) Otero Areán, C.; Tsyganenko, A. A.; Manilova, O. V.; Palomino, G. T.; Mentruit, C. P.; Garrone, E. *Chem. Commun.* **2001**, 455.
(57) Otero Areán, C.; Tsyganenko, A. A.; Platero, E. E.; Garrone, E.; Zecchina, A. *Angew. Chem., Int. Ed.* **1998**, *37*, 3161.
(58) Zecchina, A.; Lamberti, C.; Bordiga, S. *Catal. Today* **1998**, *41*, 169.
(59) Bucko, T.; Benco, L.; Hafner, J. *J. Chem. Phys.* **2003**, *118*, 8437.
(60) van Bokhoven, J. A.; van der Eerden, A. M. J.; Koningsberger, D. C. *J. Am. Chem. Soc.* **2003**, *125*, 7435.
(61) Ewing, G. E. *J. Chem. Phys.* **1962**, *37*, 2250.
(62) Gabova, V.; Dedecek, J.; Cejka, J. *Chem. Commun.* **2003**, 1196.
(63) Demuth, T.; Benco, L.; Hafner, J.; Toulhoat, H. *Int. J. Quantum. Chem*. **2001**, *84*, 110.
(64) Fricke, R.; Kosslick, H.; Lischke, G.; Richter, M. *Chem. Rev.* **2000**, *100*, 2303.
(65) Karge, H. G.; Bayer, K. H. Zeolite Chemistry and Catalysis. In *Proceedings of the International Symposium*; Prague, 1991; Jacobs, P. A., Jaeger, N. I., Kubelkova, L., Wichterlova, B., Eds.; Elsevier: Amsterdam, 1991; p 43.
(66) Karge, H. G. Zeolites and Microporous Crystals. In *Proceedings of the International Symposium on Zeolites and Microporous Crystals*; Nagoya, Japan, 1993; Hattori, T., Yashima, T., Eds.; Kodansha Ltd. and Elsevier: Tokyo and Amsterdam, 1994; p 135.
(67) Karge, H. G. *Stud. Surf. Sci. Catal*. **1994**, *83*, 135.
(68) Otero Areán, C.; Bonelli, B.; Palomino, G. T.; Safont, A. M. C.; Garrone, E. *Phys. Chem. Chem. Phys*. **2001**, *3*, 1223.
(69) Kazansky, V. B.; Borovkov, V. Y.; Serikh, A. I.; van Santen, R. A.; Anderson, B. G. *Catal. Lett.* **2000**, *66*, 39.